PNAS RESEARCH ARTICLE | BIOPHYSICS AND COMPUTATIONAL BIOLOGY OPEN ACCESS

Deciphering the underlying mechanisms of the pharyngeal pumping motions in *Caenorhabditis elegans*

Dana Sherman[a] and David Harel[a,1]

Contributed by David Harel; received February 16, 2023; accepted December 29, 2023; reviewed by Yuval Dor, Sol Efroni, and Christopher Fang-Yen

The pharynx of the nematode *Caenorhabditis elegans* is a neuromuscular organ that exhibits typical pumping motions, which result in the intake of food particles from the environment. In-depth inspection reveals slightly different dynamics at the various pharyngeal areas, rather than synchronous pumping motions of the whole organ, which are important for its effective functioning. While the different pumping dynamics are well characterized, the underlying mechanisms that generate them are not known. In this study, the *C. elegans* pharynx was modeled in a bottom–up fashion, including all of the underlying biological processes that lead to, and including, its end function, food intake. The mathematical modeling of all processes allowed performing comprehensive, quantitative analyses of the system as a whole. Our analyses provided detailed explanations for the various pumping dynamics generated at the different pharyngeal areas; a fine-resolution description of muscle dynamics, both between and within different pharyngeal areas; a quantitative assessment of the values of many parameters of the system that are unavailable in the literature; and support for a functional role of the marginal cells, which are currently assumed to mainly have a structural role in the pharynx. In addition, our model predicted that in tiny organisms such as *C. elegans*, the generation of long-lasting action potentials must involve ions other than calcium. Our study exemplifies the power of mathematical models, which allow a more accurate, higher-resolution inspection of the studied system, and an easier and faster execution of in silico experiments than feasible in the lab.

C. elegans | pharynx | pumping | muscle dynamics | mathematical model

Significance

In this study, we have constructed a mathematical model of the pharynx—the feeding organ of the nematode *Caenorhabditis elegans*—in order to analyze in detail the way pharyngeal motions are generated. Our model provides a detailed explanation of the way the pharynx works and allows studying the effects of its various components. The predictions of the model, as well as a few remaining inconsistencies between the model and experimental measurements, point to several promising future research directions, which could advance the understanding of this biological system. In addition, our modeling approach, together with the published code of the model and detailed solutions of its equations, should allow nonspecialists to use this kind of modeling for studying other biological systems.

The *Caenorhabditis elegans* pharynx is a double-bulbed tube, composed of a small number of cells, which include 20 muscle cells (Fig. 1; 1). Anatomically, the muscle cells can be divided into eight types due to threefold radial symmetry of most of them around the center of the pharynx. Functionally, they can be divided into three groups, such that within each group, all muscles contract and relax in synchrony, as if they were a single cell: a) corpus muscles: pharyngeal muscles 1-4 (pm1-4), b) isthmus muscles: pm5, and c) terminal bulb (TB) muscles: pm6-8.

All pharyngeal muscles (pm's) exhibit one of two typical motions: pumping or peristalsis. Pumping is a repetitive contraction and relaxation cycle of most of the organ. Pumping of the anterior pharynx, i.e., pm1-4 and the anterior part of pm5, sucks in bacterial food from the environment, and pumping of the posterior part, i.e., pm6-8, crushes the food and pushes it into the intestine. Peristalsis is an anterior-to-posterior wave of local contractions and relaxations along the nonpumping pharyngeal segment, i.e., the posterior part of pm5. It occurs once in every 3 to 4 pumps on average, at the end of a pump cycle (2). This study focuses on analyzing pumping dynamics (i.e., excluding peristalsis, see "*Materials and Methods*").

Inspecting pumping dynamics in detail reveals a more complicated picture than perfectly synchronized contractions and relaxations of the different pharyngeal areas (Table 1; 3–10). These include: 1) different contraction onset times of the corpus, anterior isthmus (AI) and TB; 2) different contraction-spreading speed along different pharyngeal areas: while corpus and TB contraction occurs simultaneously throughout their length, such that each contracts as one unit, contraction spreads slowly along the isthmus, within several tens of milliseconds, in an anterior-to-posterior wave; 3) different contraction-strength progression dynamics at different pharyngeal areas: while the corpus contracts gradually throughout the pump—weakly at the beginning and reaching maximum contraction toward its end, the TB reaches maximum contraction very early after pump onset, and remains at maximum contraction throughout the pump.

While the various pumping dynamics are well characterized, there is currently no explanation for the way these variations could be obtained at the different pm's. Come to

Author affiliations: [a]Department of Computer Science and Applied Mathematics, Faculty of Mathematics and Computer Science, The Weizmann Institute of Science, Rehovot 76100, Israel

Author contributions: D.S. performed research; D.S. analyzed data; D.H. managed and supervised all stages of the project; and D.S. and D.H. wrote the paper.

Reviewers: Y.D., Hebrew University of Jerusalem; S.E., Bar-Ilan University; and C.F.-Y., The Ohio State University.

The authors declare no competing interest.

[1]To whom correspondence may be addressed. Email: dharel@weizmann.ac.il.

This article contains supporting information online at https://www.pnas.org/lookup/suppl/doi:10.1073/pnas.2302660121/-/DCSupplemental.

Published February 5, 2024.

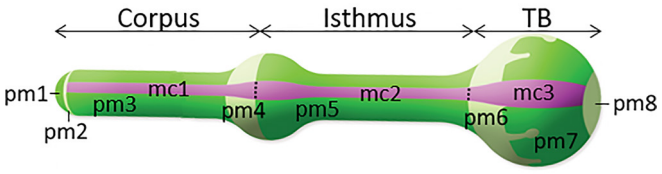

Fig. 1. *C. elegans* pharynx anatomy. In all figures, anterior is to the left, and dorsal is up. The pharynx is composed of 20 muscle (shades of green), 9 structural (named marginal; purple), and several other cells (not shown). All types of pharyngeal muscle cells (pm; 8 types), except pm1 and pm8, and all types of marginal cells (mc; 3 types) are arranged in threefold symmetry around the pharyngeal lumen, where pm1-4 and mc1 constitute the anterior part of the pharynx—the corpus; pm5 and mc2 its middle part—the isthmus; and pm6-8 and mc3 its posterior part—the TB. Adapted from ref. 1.

think of it, the variations in pumping dynamics are puzzling since they do not accord with the rather uniform dynamics of the underlying processes that lead to them: depolarization (DP) of the muscles, which induces elevation of intracellular calcium ions, which in turn induces muscle contraction. Specifically, as most data are available for the easier-to-measure DP process, if pm's pumping dynamics tightly followed those of pm's DP, which spreads rapidly, almost simultaneously throughout the organ, they should have contracted nearly synchronously and would have then exhibited similar contraction dynamics (Fig. 2; 3).

In this paper, we propose comprehensive mechanisms that explain the various dynamics measured at the different pumping areas. By accurately modeling the biological processes that underlie pm's dynamics, we were able to simulate and analyze in detail the emerging pharyngeal motions and to inspect the postulated mechanisms. Furthermore, the flow of fluid and particles through the pharyngeal lumen, which is dictated by pm's dynamics, was also modeled and compared to particles motion measured in nematodes. This allowed us to inspect the influence of simulated muscle dynamics on the emerging particles motion, and to infer some alternative pm's dynamics than reported, in a reverse engineering manner. Our model supports a functional role of the marginal cells, which are currently thought to mainly serve as structural cells, and provides a fine-resolution description of the dynamics of the pumping pm's.

Materials and Methods

The Biological Model.

The pharyngeal muscle cells. Of the several types of cells that compose the *C. elegans* pharynx, only the pm cells were modeled (Fig. 1). Since the pm's are electrically coupled within each pharyngeal area (via marginal cells; 1), and due to their threefold symmetry, only one cell was modeled for each type of muscle, where pm1-2, as well as pm6-8, were modeled by a single muscle cell that represented their collective activity (Fig. 3). Each muscle cell was assumed to occupy one-third of the volume of its corresponding pharyngeal area. The different pm's were assumed to have similar properties (i.e., similar parameter values), unless experimental data or model's output supported heterogeneity. Generally, the electrophysiological and calcium-dynamics properties of different pm's were similar, while many of their biomechanical properties varied. In order to obtain a smooth, continuous motion at the transition points between adjacent pm's in cases of heterogeneity in properties, transition areas were defined (Fig. 3). Their position and range were set based on model's output (*SI Appendix*, Table S2).

The marginal cells. While the anatomical properties of the marginal cells (mc's) were not modeled, we did model their putative functional properties, where the mc's were assumed to relay electrical signals ("*Results*"). Similar to pm's modeling, due to mc's electrical coupling within each pharyngeal area (via pm's; 1), and due to their threefold symmetry, the properties of only three mc's were modeled: mc1 at the corpus, mc2 at the isthmus, and mc3 at the TB (Fig. 1).

The modeled dynamics. The dynamics of the biological processes that underlie and lead to pharyngeal pumping were modeled (Table 2): 1) generation and propagation of an electrical signal (action potential), 2) intracellular calcium concentrations, and 3) contraction and relaxation of the pm's. Action-potential (AP) dynamics, induced by changes in transmembrane potential (V_m), were modeled using the cable equation, assuming that the changes in V_m resulted from the activity of three plasma membrane's ion channels: CCA-1, EGL-19, and EXP-2 (16), whose kinetics were modeled by the Hodgkin and Huxley equations (*SI Appendix*, Figs. S3–S13). In addition, a linear ohmic leak-current channel was modeled (16). AP generation was assumed to initiate by the firing of the MC neurons (3, 11–13), where the MC's themselves were not modeled, and their firing was modeled as an external electrode current, injected at the corpus–isthmus border (Fig. 2). No other pharyngeal neurons were modeled (*SI Appendix*). Calcium concentrations were calculated in two regions: at a thin region, ~0.2 μm deep, just beneath the cytoplasmic membrane, termed Ca_{shell}, which was assumed to affect the channels dynamics, and at the inner cell's region, occupying the bulk of the rest of the cell where the myofilaments reside, termed Ca_{cell}, which was assumed to affect pm's dynamics. A homogenous concentration was assumed within each region. Calcium influx from the plasma membrane channels was assumed to be sufficient for evoking muscle contraction (17, 18). Finally, muscle dynamics were modeled using a modified four-state latch-bridge smooth muscle model, assuming length-dependent bonding and unbonding rates. The pm's were modeled as contractile elements (CE), connected both in parallel and in series with passive elastic elements (PE and SE, respectively), and interconnected by orthogonal elements (OE). PE was modeled as a linear spring connected in parallel to a linear damper, and SE and OE were modeled as linear springs (*SI Appendix*). The muscles' filaments were assumed to be radially oriented so that when they contract, the pharyngeal lumen opens. In addition to the aforementioned processes, the flow of fluid and particles along the pharyngeal lumen was also modeled (Table 2 and *SI Appendix*).

The posterior isthmus. The dynamics of all of the pharyngeal areas were modeled, excluding those of the posterior isthmus, for several reasons (*SI Appendix*). Thus, our model's results regard pumping motions only, of all pumping areas, where the posterior isthmus remained closed (by setting its calcium-removal dynamics to be very rapid, *SI Appendix*, Table S3). Except for the calcium removal rate, similar calcium dynamics were assumed throughout the simulated pharynx.

Table 1. Contraction–relaxation dynamics of the pharyngeal areas

Motion	Property	Corpus	AI	Posterior isthmus	TB
Contraction	Onset time	0	72.7 ± 36.4 28.5 ± 14.8	~150	A few ms 38.1
	Strength progression	Gradual			Rapid
	Total time	159 ± 1 145 ± 32.3 109.7 ± 19.6	91.9 ± 30.3 94.6 ± 18.1		173 ± 2 91.4 ± 13.6
	Relaxation	Onset time	0	~20 13.4 ± 9.9	
Total time					

Onset times are relative to those of the corpus. Contraction-spreading speed refers to contraction's spatial propagation dynamics along the pm. Gradual (rapid) contraction-strength progression refers to contraction's temporal dynamics, reaching maximum contraction just before (long before) relaxation onset time. The values indicated are either mean ± STD or mean. For some dynamics, more than one value is indicated, in cases in which several values were found in the literature.

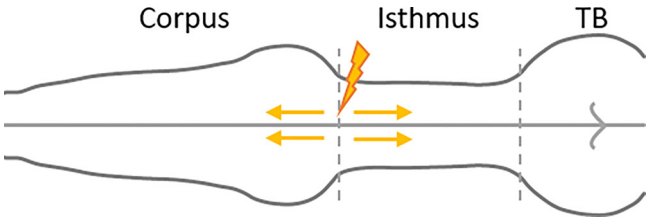

Fig. 2. Spatial dynamics of pharyngeal muscles' depolarization. Depolarization is initiated locally at the corpus–isthmus border, due to the firings of a pair of pharyngeal neurons, the MC's (lightning; 11–13), and then propagates rapidly from one pm to another due to a tight electrical coupling (arrows; 1, 3, 5, 14, 15).

In silico experiments. 1) Flattened metacorpus. The effect of pharyngeal shape on particles flow was tested by flattening the metacorpus bulb. The outer radius of the pharynx was changed manually, and a minimal set of parameters was changed in order to obtain similar particles motions (see *FLAT_META_CO* in *SI Appendix*, Table S1). 2) Changing the injection site of the external current. The effect of the position of the externally injected current on particles flow was tested by moving the injection site to the anterior tip of the pharynx, and a minimal set of changes was performed in order to obtain similar particles motions (see *EX_INPUT_NODE* in *SI Appendix*, Table S1).

The Mathematical Model. Each of the biological processes that lead to pumping was described mathematically by a partial differential equation (PDE), which was solved using the finite-element method. All PDEs and their detailed solutions are elaborated in *SI Appendix* in order to allow nonspecialists to use this kind of approach.

The finite-element mesh of the pharynx. Mechanically, the pharynx is a very rigid structure–during contractions its inner lumen opens, while its outer shape does not change (1, 16, 24). Thus, two vectors were used for describing its geometry–an outer radii vector, R, defining its outer, fixed contour, and an inner radii vector, z, describing the changing contour of the lumen (*SI Appendix*, Fig. S20). R was set based on morphological data of an adult *C. elegans* nematode (25, *SI Appendix*, Fig. S1). z was calculated using the muscles' PDE. For this purpose (and for V_m and calcium calculations), the pharynx was divided along its x-axis into equal-length segments, specified by a series of points. Each segment was further divided along its z-axis into a submembrane region and an inner cell region, respectively for Ca_{shell} and Ca_{cell} calculations (*SI Appendix*, Fig. S20).

Fitting of model parameters. The values of all model's parameters (elaborated in *SI Appendix*) were initially set to best fit experimental data, when available. Since this initial fitting did not result in the desired AP, muscle, and particle dynamics, we tested the effect of changing the values of various parameters. Using a genetic algorithm that we developed, a range of values was inspected for each parameter, and when either the emerging AP's shape, muscle dynamics, or particles flow greatly improved, the initial parameter's value was changed. Since all biological processes affected each other and ultimately the resulting particles flow, we prioritized changes that improved fitting to the following data, mentioned from top to lowest priority: 1) particles flow data, 2) (widely available) AP data, and 3) low-level (partial) data of ion channels and (low temporal and spatial resolution) pm's-dynamics data.

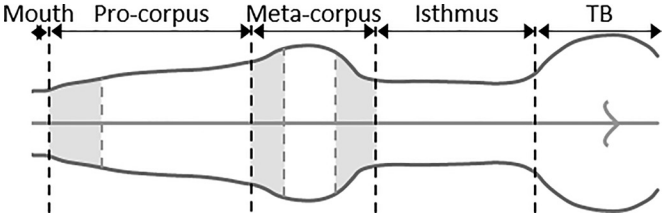

Fig. 3. Pharyngeal and transition areas in the model. Five pm cells were modeled: "mouth," procorpus, metacorpus, isthmus, and TB cell, representing pm1-2, pm3, pm4, pm5, and pm6-8, respectively. Transition areas (gray shaded) between adjacent pm's were defined in order to set a gradual change in the values of parameters that varied between different pm's.

Results

Modeling Pharyngeal Muscles' Action Potential. The *C. elegans* pharyngeal muscles (pm's) exhibit repetitive, characteristic action potentials (APs), generated by the activity of three main ion channels: CCA-1, EGL-19, and EXP-2 (Fig. 4 and Table 3; 16). Channels activity is triggered by pm's DP, which is initiated by the activity of the MC neurons (Fig. 2; 11–13). In our model, MC's activity elevated the membrane potential (V_m) from a resting potential of −73 ms to about −40 mV (Fig. 5*A* and *SI Appendix*, Table S1). This activated the ion channels, which resulted in the generation of an AP. The modeling and analysis of the simulated AP was done by comparing the properties of the modeled ion channels, and of the emerging AP, to those measured in the nematode, as elaborated upon below.

The CCA-1 channels are T-type voltage-gated calcium channels that give rise to a large, quickly inactivating inward current, which drives rapid, transient membrane DP. Their activation voltage is ~−40 mV, and their current peaks at ~−30 mV (16, 32, 33). The EGL-19 channels are L-type voltage-gated calcium channels, which activate at high V_m's in a long-lasting manner, and thus maintain AP's plateau. Their activation voltage is ~−10 mV, and their current peaks at ~+20 mV (16, 32, 33). The EXP-2 channels are voltage-gated potassium channels of the Kv family, which trigger rapid repolarization at the end of the plateau due to large outward currents (16, 26, 34).

In accordance with experimental data, the simulated CCA-1 currents were large and transient (Fig. 5 *B* and *C*), and their activation voltage was ~−40 mV (*SI Appendix*, Figs. S2 and S3). In addition, they were necessary for a smooth, steep rise in V_m after pm's DP by MC's firings: In their absence, no AP was generated, and V_m reached ~−40 mV, in accordance with reported data (Fig. 5*A*; 28). In contrast to data, the simulated CCA-1 currents were adjusted to peak at a higher voltage of −20 mV since setting their peak at −30 mV did not allow generating APs with the desired characteristics (see "*Fitting of model parameters*" in "*Materials and Methods*" and *SI Appendix*, Fig. S2).

Similar to measurements, the simulated EGL-19 currents lasted for a long period of time (Fig. 5 *B* and *C*), their activation voltage was −10 mV, and they peaked at +20 mV (*SI Appendix*, Fig. S8). In accordance with data, they participated in the AP's rising phase (28, 30, 31), and were necessary for maintaining the plateau: When absent, the maximal upstroke rate and peak amplitude were smaller (13.7 mV ms^{-1} and 28.7 mV, respectively), while no plateau was generated (Fig. 5*A*).

In accordance with measurements of EXP-2 currents, large outward potassium currents were generated at the end of the simulated AP, and were necessary for hyperpolarizing V_m to −80 mV (Fig. 5 *A* and *B*). Similar to the nematode, the simulated EXP-2 currents could not be generated during the depolarizing phases of the AP due to channel's ultrafast inactivation upon DP (*SI Appendix*, Fig. S12).

The dynamics of the simulated CCA-1 and EGL-19 channels described so far were obtained when assuming that these channels relayed both calcium (Ca^{2+}) and sodium (Na^{+}) ions. When assuming that CCA-1 and EGL-19 were permeable to Ca^{2+} alone, the desired AP could not be generated by our model: CCA-1 channels exhibit very large currents (16). Permeability to Ca^{2+} alone required extremely large currents for elevating V_m, which also rapidly decreased calcium's reversal potential (E_{Ca}), preventing V_m from reaching its desired peak value. The lower V_m, which could not cross +4 mV, left the CCA-1 channels open, which, due to their large Ca^{2+} current, kept E_{Ca} at ~0 mV throughout the plateau (Fig. 6*A*).

Table 2. Modeling methods of the underlying processes of the pharyngeal pumping motions

Process	Modeling method	Description	Rerence work
Electrical signal	Cable equation	Spread of electrical signal over time and space	(19)
	Hodgkin–Huxley equations	Change of electrical signal over time due to ion channels activity	(20)
Calcium dynamics		Change of calcium ion concentration over time and space, due to ion channels activity, ion removal processes, and ion diffusion	(21)
Muscle dynamics	Nonisometric kinetic model for smooth muscles	Change of pharyngeal muscle's length over time due to active and passive forces exerted by biomechanical elements	(22, 23)
Food transport along the pharynx	Low Reynolds number internal flow equations	Fluids flow	(6)

We therefore postulated that the CCA-1 channels might be permeable to an additional ion other than Ca^{2+}. Of the most common ions that flow across ion channels—N^+, K^+, Ca^{2+} and Cl^-—N^+ seemed to best fit since its electrochemical gradient widely promotes DP, while not changing the reversal potential (like all ions besides Ca^{2+}). Assuming CCA-1 permeability to both Ca^{2+} and Na^+ allowed generating a rapid membrane DP at the desired rate, but one that could not cross +28 mV. In addition, the resulting AP plateaued around ~0 mV since now the large EGL-19 Ca^{2+} currents that were required for inducing a long-lasting DP rapidly decreased E_{Ca} to ~0 mV (Fig. 6*B*).

We therefore tested the possibility of EGL-19 permeability to both Ca^{2+} and Na^+. Assuming EGL-19 permeability to both ions, and CCA-1 permeability to Ca^{2+} alone, resulted in a rapid membrane DP at the desired rate, but one that could not reach the desired +34 mV, and which did not display the notch observed in nematodes. In addition, the resulting AP plateaued around ~+15 mV or below (Fig. 6*C*). Alternatively, assuming that both CCA-1 and EGL-19 relayed both Ca^{2+} and Na^+, allowed the generation of a rapid membrane DP at the desired rate, and to the desired peak voltage. The resulting AP displayed a notch, and plateaued around ~+25 mV for the desired period of time (Fig. 5*A* and Table 3). Under these conditions, the Na^+ currents of both channels were 1 to 2 orders of magnitude larger than their corresponding Ca^{2+} currents (Fig. 6 *B* and *C*).

Sodium dependency of AP generation stemmed from the small size of the pharynx, which is in the micrometer scale (1, 6): When assuming either CCA-1 or EGL-19 permeability to Ca^{2+} alone, the large Ca^{2+} currents increased submembrane Ca^{2+} concentration (Ca_{shell}) by five orders of magnitude due to the small volume of the pharyngeal cells. This, in turn, decreased E_{Ca} to ~0 mV, which is way below the desired peak or average plateau's potentials. Increasing pharyngeal size by two orders of magnitude or more allowed generating APs by Ca^{2+} currents alone since at these conditions, Ca_{shell} peaked to lower levels, which allowed keeping E_{Ca} above the desired +34 mV throughout the AP (Table 4).

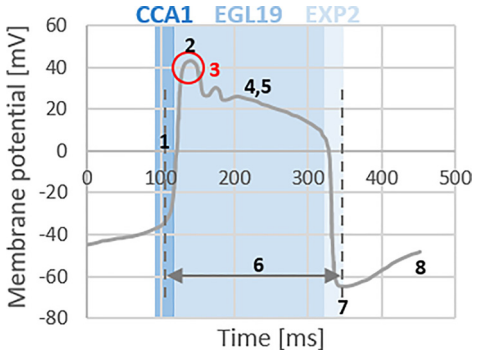

Fig. 4. Temporal dynamics of pharyngeal muscles' action potential. The AP can be divided into three phases: rising (dark blue), plateau (blue), and repolarization (light blue), generated, respectively, by the activity of CCA-1, EGL-19, and EXP-2. The AP shape can be quantified by a set of parameters (numbered), whose corresponding values are listed in Table 3. Adapted from ref. 26, using WebPlotDigitizer (27). Reprinted with permission from AAAS.

Modeling Calcium Dynamics. In contrast to the well-studied pm's AP, much less data are available regarding Ca^{2+} dynamics (9, 35, 36), and these are not as accurate: Ca^{2+} levels are measured indirectly, by low-sensitivity and slow-kinetics sensors, which often themselves alter the dynamics (21, 37). Hence, the following description and analysis of the simulated Ca^{2+} dynamics are much more laconic.

Simulated intracellular calcium (Ca_{cell}) dynamics at the different pharyngeal areas were generally similar throughout the pharynx (except for a rapid and continuous reduction of Ca^{2+} to basal levels at the posterior isthmus, see "*Material and Methods*"), in accordance with experimental data (35). In our model, Ca_{cell} elevation started shortly (~40 ms) after AP onset (Fig. 7 *A–D*). The simultaneous Ca_{cell} elevation stemmed from the rapid spreading of the simulated AP along the pharynx, which occurred within a few milliseconds (3). Different from similar Ca_{cell} elevation onset times, initial (at ~40 ms) and maximal (at ~190 ms) Ca_{cell} levels differed between segments, stemming from variations in pharynx geometry (Fig. 7*E*).

The temporal dynamics of the simulated Ca_{cell} fitted experimental data only partially (35): In our model, Ca_{cell} elevated from basal to maximal levels within ~150 ms and returned to basal levels within ~200 to 300 ms (Fig. 7 *A–D*). These dynamics fit quite well the dynamics measured at high-frequency pumping but are inconsistent with much slower dynamics measured at low-rate pumping (*SI Appendix*, Figs. S14 and S15). Setting Ca_{cell} dynamics that fitted low-rate pumping did not allow fast and large-enough muscle relaxation for successfully catching food particles, and hence high-rate pumping dynamics where set (see "*Fitting of model parameters*" in "*Materials and Methods*").

Modeling Pharyngeal Muscles and Particles Dynamics. According to Table 1, it is obvious that at least the AI does not start contracting concurrently with the corpus and TB, but rather after a long delay [Electropharyngeogram (EPG) data (38, 39), which reflect pm's electrical activity, and video-recording analyses of pm's contraction times (10), conflictingly support of a near-simultaneous and an asynchronous contraction of the corpus and TB muscles, respectively; Table 1]. In addition, the AI contracts slowly from anterior to posterior (3). When assuming that pm's dynamics were governed by Ca_{cell} dynamics alone, the desired AI dynamics could not be generated by our model since simulated Ca_{cell} elevated simultaneously throughout the pharynx (Fig. 7). We thus postulated that a factor other than Ca^{2+} might control pm's dynamics. Consistent

Table 3. Comparison of the quantitative properties of the simulated APs to those generated by the pharyngeal muscles

	Parameter	Nematode	Model	Experimental data
1	Maximal rate of upstroke [mV ms^{-1}]	15 ± 1	14.6	(28)
2	Peak amplitude [mV]	34 ± 3	34.6	(3, 16, 29, 30)
3	Notch exists?	v	v	
4	Average potential of plateau [mV]	~20 to 30	25	(3, 26, 28, 29)
5	Average decrease rate of plateau [mV ms^{-1}]	−0.22 ± 0.06	−0.1	(16)
6	Action potential total duration [ms]	100 to 250	~175	[16, 28 (WPD), 29, 30]
7	Action potential overshoot [mV]	~−80 (−67 ± 1.5)	−80	[28 (WPD), 29]
8	Average interpump potential [mV]	−73 ± 1 (−45 ± 1)	−73	[3, 28 (WPD), 29, 30, 31]

All values were inferred from intracellular recordings from TB muscles. Experimental data for parameters 7 and 8 suggest two possible values, where the nonchosen, alternative value is written in brackets. WPD—WebPlotDigitizer (27).

with this idea, in smooth muscles, such as the pm's (24), Ca^{2+} is a necessary factor for inducing contraction, yet another factor, a signal-transduction-activated contraction-inducing factor (CF), can regulate it (*SI Appendix*, Fig. S24). If such a CF could be activated at different pm's with different delays following Ca_{cell} elevation, this could have explained the measured variability in pm's contraction onset times, and specifically the large latency in AI contraction. Furthermore, if CF activation could occur in a gradual and local manner along the pm's, this could have explained the gradual AI contraction.

While several signal transduction pathways could potentially enhance pm's contraction, an explicit pathway with a specific CF is yet to be found. Yet, assuming that such a CF acts at the pm's, then regardless of its identity, its activation should be delayed relative to Ca_{cell} elevation (*SI Appendix*, Fig. S24). In order to explain a gradual activation of the CF along the isthmus, we postulated that the signal transduction started at external structures that stretched along the entire isthmus muscles. Such structures should relay the signal slowly, and activate the CF locally, influencing small muscle segments separately.

Anatomically, two types of cells may fulfill these requirements: several types of pharyngeal neurons and the marginal cells (mc's). Functionally, while none of the pharyngeal neurons fit, the mc's seem to be good candidates (*SI Appendix*). We thus added an arbitrary CF to our model, without modeling its upstream pathway, and set its dynamics in a top-down fashion (in contrast to all other model's dynamics, which emerged in a bottom–up fashion; *SI Appendix*, Tables S5 and S6). Spatially, the external CF-activating signal was assumed to spread gradually from the corpus–isthmus border toward both edges of the pharynx via the mc's, and to activate the CF locally (Fig. 8*A*). The mc2's were assumed to convey the signal more slowly than the mc1's and mc3's, for inducing a more gradual contraction. Temporally, the external signal was assumed to act rapidly, on the scale of milliseconds, triggering a fast, temporary activation of the CF (Fig. 8 *B*–*E*). While CF-activation dynamics were the major factor that determined pm's dynamics in our model, several calcium parameters also affected them, where the dissociation constants of MLCK and MLCP from Ca^{2+} were the second major factor (*SI Appendix*, Table S4). These constants will be termed here "Ca_{cell} thresholds."

Contraction dynamics of all simulated pm's were similar: Contraction started once Ca_{cell} levels crossed a certain threshold (at ~50 to 70 ms; different Ca_{cell} thresholds were set for different pm's, *SI Appendix*, Table S4), and became significantly stronger upon CF activation (at ~100 ms, Figs. 7–9). Accordingly, at the beginning of a pump the pharyngeal lumen opened to a lesser extent, followed by a more rapid and wider opening. Relaxation dynamics of all pm's were also similar: Once CF activation stopped, muscle contraction no longer continued, while relaxation started once Ca_{cell} levels dropped below a certain threshold (at ~200 to 250 ms; different Ca_{cell} thresholds were set for different pm's, *SI Appendix*, Table S4). The opening and closing of the pharyngeal lumen resulted in particles flow along the pharynx (Fig. 10). As mentioned, the emerging particles flow was used to infer the dynamics of the pm's, and its fitting to measurements was favored over the fitting of pm's dynamics in cases of a conflict, as elaborated upon below. Hence, in the following subsections, the simulated

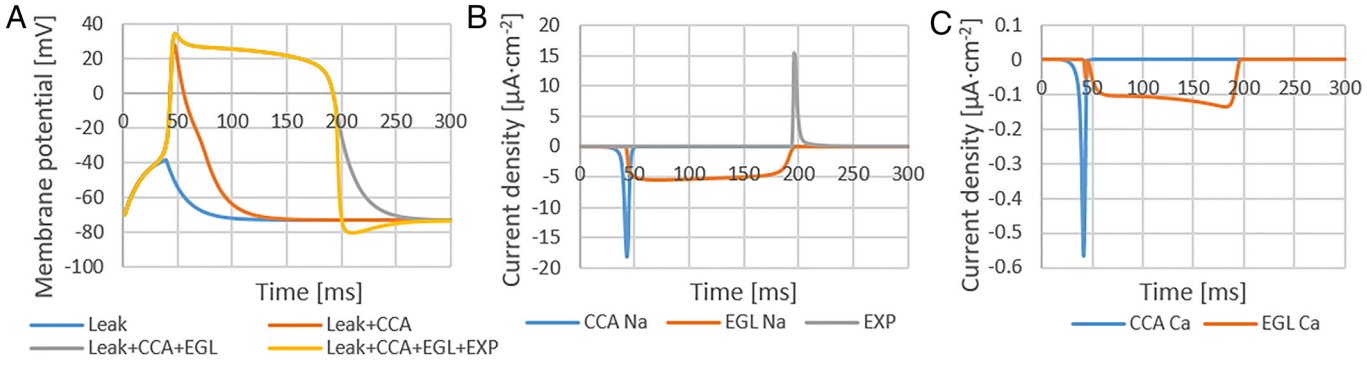

Fig. 5. Simulated membrane potential and its underlying currents. (*A*) The pm's AP could not be generated by CCA-1 (orange) nor EGL-19 (blue) currents alone. The EXP-2 current accelerated membrane hyperpolarization at the end of the AP (yellow vs. gray). Leak currents alone, or leak currents together with EGL-19 currents, resulted in similar changes in V_m (blue). (*B* and *C*) The currents that underlie the pm's AP (*A*, yellow). Sodium (*B*) and calcium (*C*) currents are shown separately due to different scales. All data were measured from the widest point of the metacorpus (graphs are almost completely identical throughout the simulated pharynx, i.e., all pharyngeal regions exhibited similar and concurrent DP and repolarization dynamics).

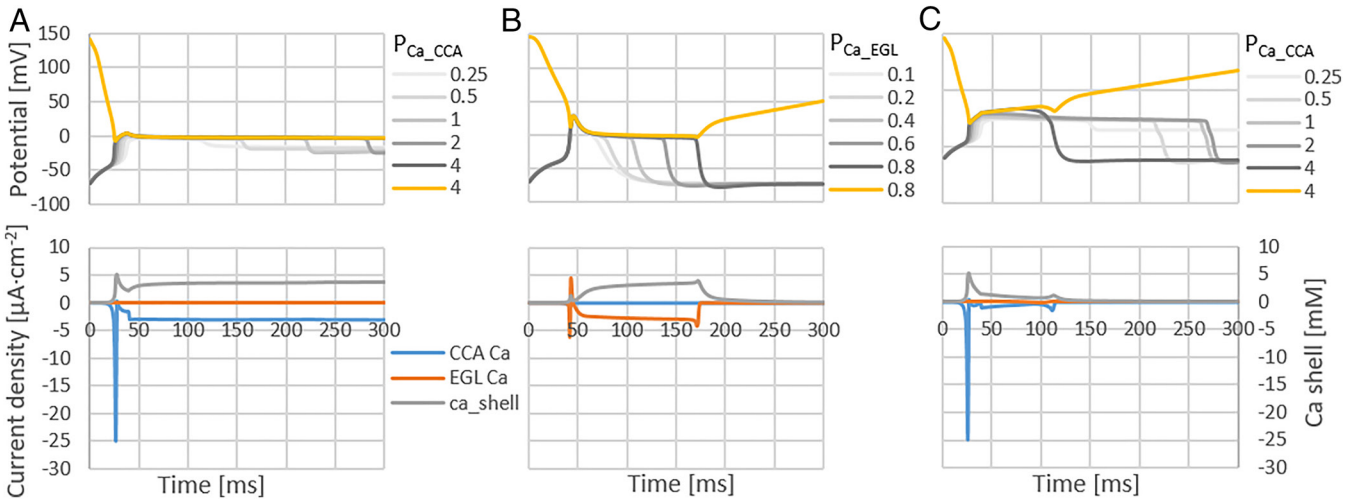

Fig. 6. Simulated membrane potential and its underlying currents, generated when zeroing Na^+ permeability. (*A–C*) Simulated V_m's (Top, gray scale) generated at different Ca^{2+} permeabilities (P_{Ca}'s), when zeroing Na^+ permeability of both CCA-1 and EGL-19 channels (*A*), of EGL-19 channels (*B*), and of CCA-1 channels (*C*). Ca^{2+} permeability of either the CCA-1 (P_{Ca-CCA}) or EGL-19 (P_{Ca-EGL}) channels was set to be 2 to 3 orders of magnitude larger than the best-fitting values, in an attempt to elevate V_m to +34 mV (*SI Appendix*, Table S3). The value of no other model's parameter was altered. E_{Ca} (*Top*, yellow) and calcium current densities and concentrations (*Bottom* graphs) were plotted only for the largest P_{Ca} (*Top*, darkest gray). In (*A*), increasing P_{Ca_EGL} did not affect the resulting V_m.

pm's and particles dynamics are jointly described and analyzed. An animation of all of the simulated dynamics is provided in order to allow visualizing all of the modeled dynamics in an integrative manner (Movie S1).

Corpus Dynamics. Simulated corpus muscles' dynamics were similar to measurements (Fig. 9 *A* and *B*): The corpus opened quite simultaneously throughout its length, within 9 ms, where its lumen gradually opened throughout the pump, reaching maximal opening just before relaxation onset (3, 5). Its total contraction time ranged between 144 and 165 ms, in agreement with measurements (159 ± 1; 145 ± 32.3 ms). Corpus relaxation was also relatively synchronous throughout its length, within 24 ms, where its lumen closed within 21 to 67 ms, in partial agreement with measurements (35.4 ± 7.1; 34.8 ± 11 ms).

Besides the reported pm's dynamics, the emerging simulated particles flow had to accord with the following observations, and hence several adjustments were made: 1) Particle 4 intake starts 10 ms before particle 3 intake (Fig. 10). This implies a posterior-to-anterior opening of the corpus. While these dynamics accord with those of CF activation and hence with those of late corpus contraction, the initial opening of the corpus already untrapped particles 3 to 4, where it (rapidly) propagated from anterior to posterior due to a corresponding decrease in initial Ca_{cell} levels (Figs. 7 *A* and *B*, 8 *B* and *C*, and 9 *A* and *B*). Setting different Ca_{cell} thresholds at the mouth (highest), procorpus, and metacorpus (lowest), allowed the desired release of particle 4 prior to particle 3; 2) Particles 3 to 4 do not slow down when passing through the metacorpus (Fig. 10). Reducing Ca_{cell} threshold at the metacorpus reduced the slowing-down of these particles but also undesirably flattened the metacorpus lumen. The minimal threshold that still elicited a spherical opening of the metacorpus lumen was chosen, which undesirably slowed-down particles 3 to 4 (Fig. 10).

The high Ca_{cell} threshold at the mouth, together with an early cessation of CF activation and an underdamping ratio between mouth PE's spring and damper (*SI Appendix*, Tables S4 and S6), also resulted in an earlier (16 ms) closing of the mouth relative to the rest of the pharynx, in accordance with measurements (7, 10), and was necessary for successfully trapping particles 1 to 2 within the pharynx during pm's relaxation. However, the early closing of the mouth dictated a smaller opening of its lumen (to a 2.6-μm-wide diameter) than implicitly measured (≥ 3 μm; 7).

Table 4. The effect of pharyngeal size on calcium's reversal potential

Scale of pharyngeal size [m]	10^{-6}	10^{-5}	10^{-4}	10^{-3}
Ca_{shell} at AP peak [mM]	3	1.3	0.18	0.002
E_{Ca} at AP peak [mV]	0	10.6	36	93

E_{Ca} was calculated for the temperature and extracellular calcium concentration indicated in *SI Appendix*, Table S3.

Isthmus Dynamics. Similar to all other pm's, the simulated isthmus muscles exhibited a small, initial, Ca_{cell}-derived contraction (at ~60 to 70 ms), resulting in a small, initial opening of the lumen, which was followed by a delayed and more significant CF-derived contraction (at ~90 to 130 ms; Figs. 8*D* and 9*C*). While the initial contraction did not fit the measured isthmus dynamics, starting simultaneously (within 11 ms) throughout the entire isthmus, and with no delay relative to the other pharyngeal areas, the delayed contraction fitted well, with a contraction onset time of 40 to 82 ms following corpus contraction (vs. measured 72.7 ± 36.4 ms), which spread from anterior to posterior within 42 ms (vs. measured ~65 ms), and which lasted 80 to 115 ms (vs. measured 91.9 ± 30 and 94.6 ± 18.1 ms). Isthmus relaxation also fitted data with a total relaxation time of 42 to 54 ms (vs. measured 40.5 ± 11.9 and 34.9 ± 15.2 ms).

Besides the reported pm's dynamics, the emerging simulated particles flow had to accord with the following observations, and hence, several adjustments were made: 1) Particle 5 intake starts 42 ms after particle 4 intake (Fig. 10). Different from the other pharyngeal areas, the initial opening of the isthmus lumen was very small due to a high Ca_{cell} threshold (*SI Appendix*, Table S4), keeping particle 5 trapped. Thus, CF-activation dynamics could determine particle 5 intake onset time. Setting a slow mc2's relay pace that fitted the measured ~65 ms contraction propagation time (6), resulted in a postponed release of particle 5 relative to measurements (7). Hence, a faster mc2's pace was set, yielding a shorter propagation time (42 ms) than reported; 2) Similar ejection onset times of particles 1 to 5 (Fig. 10). For this purpose, the

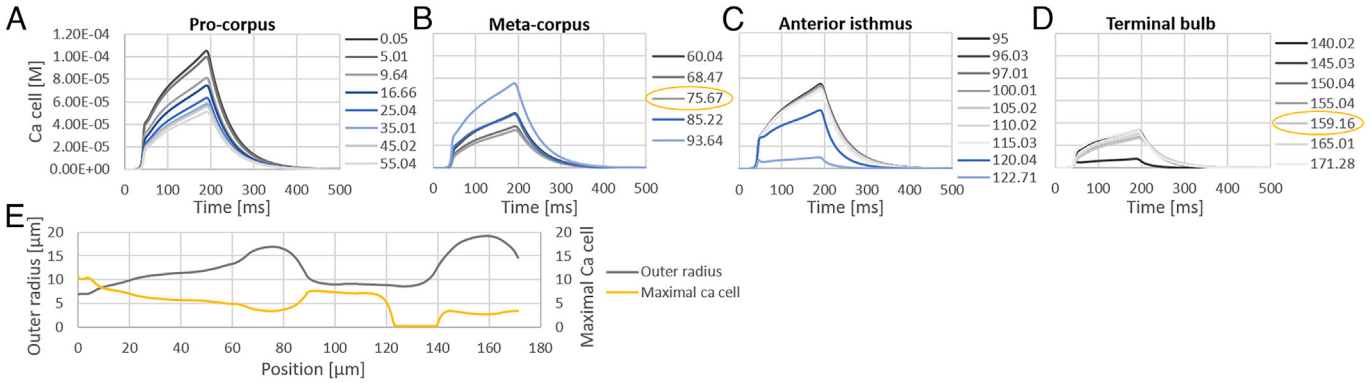

Fig. 7. Simulated Ca_{cell} dynamics at the different pharyngeal areas. (*A–D*) In Figs. 7–9, the dynamics were measured throughout a pump at various segments along the pumping pharyngeal areas. Dynamics within each area are indicated by gray-scale graphs, where those along transition regions are depicted in blue (Fig. 3). The *x*-position of the widest segment along the metacorpus and TB is encircled in yellow. (*E*) An inverse relation between outer pharyngeal radius and maximal Ca_{cell} levels (maximal Ca_{cell} [M] was multiplied by 10^5 to scale with the outer radius range).

simulated isthmus was tuned to start relaxing simultaneously with the metacorpus. While this resulted in the desired particles motion, the concurrent metacorpus and isthmus relaxation did not accord with a reported delay of ~20 ms (6, 10), which was shown to be important for a more efficient transport of food along the anterior pharynx (6, 7). Still, in support of Avery and Shtonda (6) findings, in order to successfully trap particles 3 to 4 at the simulated isthmus, its closing dynamics had to be slower than those of the corpus, which was done by setting slower CF-inhibition dynamics, and an overdamping ratio between isthmus PE's spring and damper (*SI Appendix*, Tables S4 and S6).

TB Dynamics. Unlike the radially oriented corpus and isthmus muscle filaments that open the pharyngeal lumen laterally upon contraction, some of the nematode's TB filaments are oriented obliquely to the anterior-posterior axis, resulting in a rotation motion of the TB's grinder upon muscle contraction (3). Since in our model, TB motion did not affect particles motion (due to a permanently closed posterior isthmus), all TB filaments were assumed to be radially oriented. Although the simulated TB's motion was partially different from that measured in nematodes, several aspects could be compared and analyzed (Fig. 9*D*). The simulated TB started to contract simultaneously with the corpus muscles, as supported by EPG data (38, 39), but different from video-recording analyses of pm's dynamics, which measured a ~40 ms delay between corpus and TB contraction onset times (10). In accordance with measurements, the simulated TB contracted synchronously throughout its entire length (within 5 ms), reaching maximal contraction relatively early after pump onset and remaining at maximal contraction throughout the pump (5), with a total contraction time of 177 to 186 ms (vs. measured 173 ± 2 ms). Muscle relaxation started 17 to 29 ms after the corpus, in agreement with measured delays of ~20 ms, and lasted for tens of milliseconds (55 to 62 ms, vs. measured 52.2 ± 14.5 ms). These dynamics were obtained by setting CF-activation dynamics different from those of the other pharyngeal areas, with a very early cessation of activation that allowed an early cessation in the opening of the lumen, and by setting a low Ca_{cell} threshold that resulted in a delayed and slower closing of the lumen (but also in its early opening; Figs. 8*E* and 9*D* and *SI Appendix*, Tables S4 and S6).

In Silico Experiments. The double-bulb shape of the *C. elegans* pharynx evolved from a flat-corpus ancestral shape (40). We tested whether such a geometrical change in *C. elegans* pharynx would affect the emerging particles motion (*SI Appendix*, Fig. S1), and found no significant effect (Fig. 10). We also tested whether changing the position of the injection site of the external current would affect the resulting particles flow. Injecting the external current at the anterior tip of the pharynx did not significantly change the emerging particles flow: Moving the injection site did not affect AP's dynamics, which rapidly spread along the pharynx within a few milliseconds, and inversing mc1's relaying direction (to anterior-to-posterior) had a very little effect on the resulting particles motion.

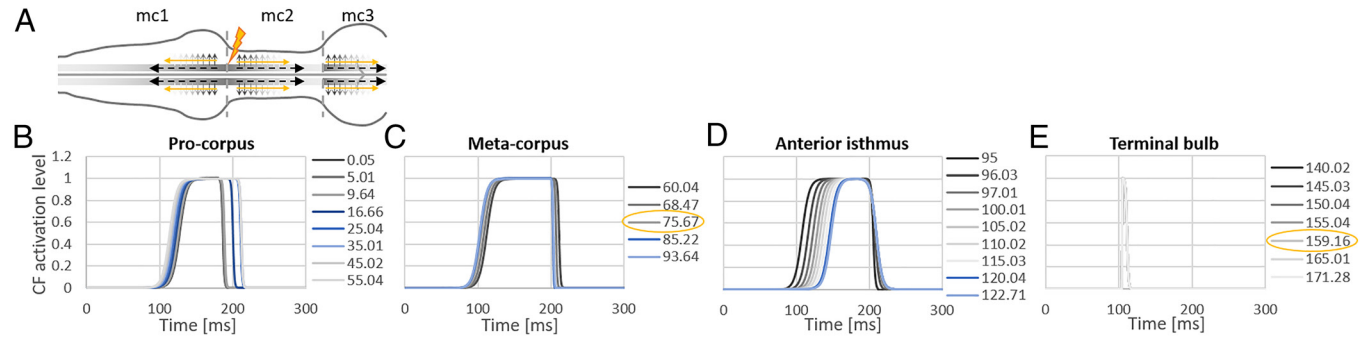

Fig. 8. CF dynamics at the different pharyngeal areas. (*A*) Spatial dynamics of the simulated CF activation. Activation was assumed to initiate at the corpus–isthmus border (lightning) and to gradually spread throughout the pharynx via the mc's. (*B–E*) Temporal dynamics of CF activation (arbitrary units).

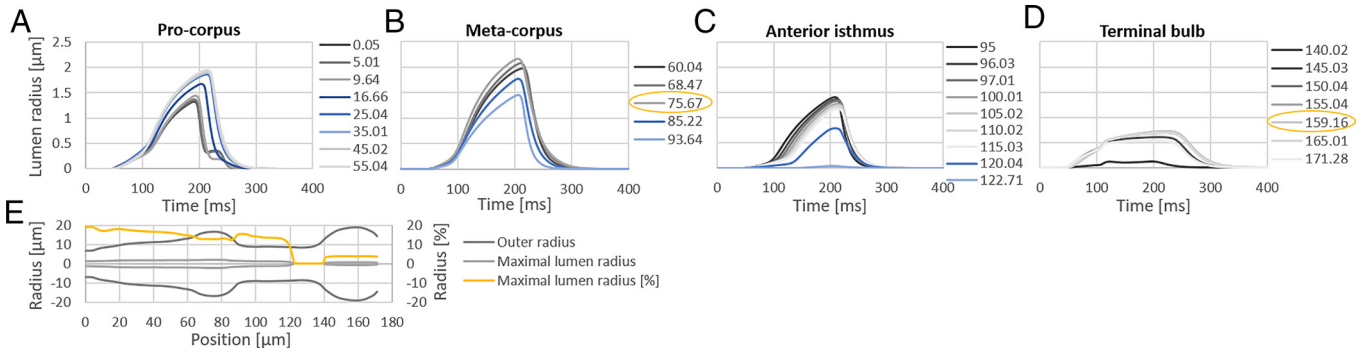

Fig. 9. Pm's dynamics at the different pharyngeal areas. (*A*–*D*) Simulated pm's dynamics, indicated by the radii of the pharyngeal lumen. (*E*) An inverse relation between pharyngeal outer radius and maximal lumen radius, where the latter is also expressed in %, relative to its corresponding outer radius.

Discussion

In this study, we modeled an entire organ, the *C. elegans* pharynx, in a bottom–up fashion, including all of the underlying biological processes that eventually lead to its end-function—the drawing in of food particles from the environment. The emerging dynamics of all processes nicely fit most measurements. Moreover, the model provides both a finer-resolution description of the various pumping dynamics than available from measurements, and some detailed explanations for their variability (Table 5). Finally, it provides a quantitative assessment of the values of many parameters that are unavailable in the literature.

Establishing an accurate model that reliably simulates the reported dynamics, at all levels of activity, allows one to further inspect the simulated system. Although two out of three in silico experiments that we conducted (changing pharyngeal size, shape, and injection site of the external current) did not provide new insights about the system, they do provide some examples for how easy and fast it is to conduct in silico experiments, within minutes, that would take years in the lab, if that is even possible at all.

Pharyngeal Muscles Repolarization. While most of the simulated dynamics fit measurements, there is an inconsistency between the two with regard to pm's repolarization and relaxation. While repolarization of all simulated pm's started simultaneously, in the nematode, corpus repolarization starts 50 ms before that of the isthmus and TB muscles (15). Similarly, while in the nematode relaxation onset time of the corpus precedes that of the isthmus, these simulated areas started to relax in synchrony (whereas both in the model and nematode the anterior tip of the corpus and the TB are, respectively, the first and last to start relaxing; 10). The concurrent relaxation in the model stems from a concurrent repolarization of all of the simulated pm's. The concurrent repolarization (and DP) stems from the assumption that they are all tightly electrically coupled by gap junctions. One possibility for explaining the difference in repolarization times of the different pm's in the nematode is Li et al. (5) suggestion, that the gap junctions found at the metacorpus and at the isthmus might rectify.

Electrical synapses can rectify, i.e., pass current preferentially in one direction, when the two sides of the junction contribute hemichannels with different properties to the gap junction (41). Since the metacorpus and isthmus exhibit two different types of innexins (14), Fig. 4), these areas could hypothetically allow a concurrent DP of all of the pm's, by allowing depolarizing currents to pass from the corpus–isthmus border to both edges of the pharynx, while also allowing different repolarization dynamics, by not passing repolarizing currents from the corpus to the TB muscles (or alternatively, by not passing depolarizing currents from the TB to the corpus). Future experiments that will examine Li et al. (5) hypothesis in the nematode should be conducted before the integration of such a mechanism in our model.

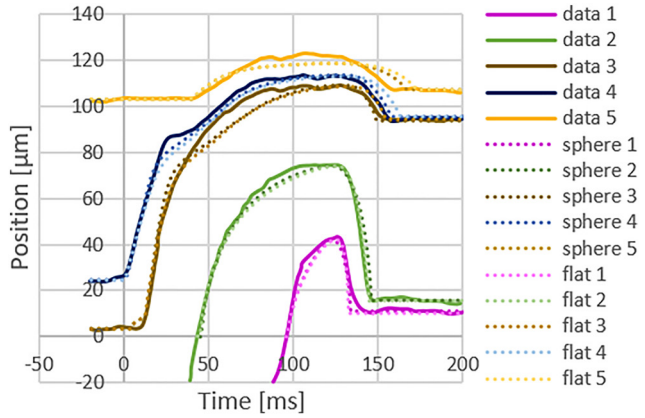

Fig. 10. Particles flow along the pharyngeal lumen during one pharyngeal pump cycle.Comparison between the trajectories of five particles measured in the nematode ["data"; adapted from ref. 7, using WebPlotDigitizer (27)], and of the corresponding simulated particles, when assuming either a spherical ("sphere") or a flat ("flat") metacorpus ("*Materials and Methods*").

Sodium Dependency of AP Generation. Our model predicts that in tiny creatures such as *C. elegans*, the generation of APs that exhibit a long, above-zero-millivolt plateau, must involve ions other than Ca^{2+}. In the *C. elegans* pharynx, our model supported the permeability of both the CCA-1 and EGL-19 channels to both Ca^{2+} and Na^{+} (Fig. 6). Other models of the pm's (e.g., refs. 21, 42, and 43) did not find such Na^{+} dependency since the Ca^{2+} currents were modeled as linear ohmic currents rather than using the more appropriate, nonlinear Goldman–Hodgkin–Katz equation, which we used. Permeability of *C. elegans* CCA-1 channels to Na^{+} was already suggested by Senatore et al. (44), while previous studies could not determine whether these channels were selective for Ca^{2+} alone (16, 30). In contrast, no experimental data support EGL-19 permeability to Na^{+}. Still, the additional permeability of either type of channels to Na^{+} accords with, and provides a possible explanation for Franks et al. (30) findings that show that extracellular Na^{+} is required for the generation of, and affects the shape of, pharyngeal APs.

A Functional Role for the Marginal Cells. The marginal cells (mc's) are understudied relative to other pharyngeal cells like neurons or muscles. The mc's are assumed to mainly fulfill a structural role,

Table 5. A summary of the dynamics predicted by the model for the different pharyngeal areas

Area	Model's prediction	Experimental data supporting prediction
Corpus	(Rapid) posterior-to-anterior opening of the lumen due to a corresponding increase in Ca_{cell} threshold	Onset time of the drawing in of particle 4 is prior to that of particle 3 (7, Fig. 3)
Corpus	Anterior-to-posterior closing of the lumen due to a corresponding decrease in Ca_{cell} threshold	Catching of particle 1 is prior to that of particle 2 (7, Fig. 3)
Isthmus	Anterior-to-posterior increasing delay in CF-activation onset time	Gradual anterior-to-posterior opening of the isthmus
Isthmus	Relaxation starts simultaneously with the corpus but is more gradual	Similar ejection onset time of particles 1 to 5 (7, Fig. 3), while slower closing is required for trapping particles 3 and 4 at the isthmus
TB	Low Ca_{cell} threshold and brief CF activation	The former postponed TB relaxation onset after that of the corpus, and the latter resulted in reaching maximal contraction early in the pump, as observed (5)

whereas it was previously suggested that they could also serve as fast conductors that excite the electrically coupled muscle cells, for achieving synchronous contractions along pm's of similar types (1, 3, 45). However, these are mostly high-level hypotheses, which we have not yet seen being tested in the nematode. Here, we postulated and examined in detail a functional role for the mc's. Our model supports the hypothesized functioning of the mc's as electrical signal relaying cells. However, in contrast to their previously suggested fast transmission, our model suggests that these cells are slow conductors, allowing some a-synchronous contractions along the muscle cells, by triggering a gradual and delayed activation of a CF. The model predicts that the CF-activation dynamics are the major factor in determining the contraction-relaxation dynamics, rather than the Ca^{2+} dynamics. Such a-synchronies, both within and between pharyngeal areas, are important for the proper functioning of the pharynx (6, 7).

Our model integrates all levels of activity that underlie the function of an organ. Such multilevel modeling has several advantages: Examining the dynamics of each of the underlying processes in a wider context can point at different dynamics than those that best fit measurements when analyzing it as a stand-alone process (i.e., when improving, in overall, the activity of the entire system), thus providing some insights about its dynamics. Moreover, it allows one to use experimental data that describe, say, one process for inferring the dynamics of other processes, and hence to gain more information from available data. Finally, the comprehensive integration of all processes allows us to obtain and analyze the emerging behavior of the organ, and hence to greatly improve the intuition and understanding of the way the system works as a whole.

Our study demonstrates the high complexity of biological systems, as exemplified even in a tiny, low-number-cell organ such as the *C. elegans* pharynx, and illustrates the importance of mathematical models: The high temporal and spatial complexities of the biological processes, together with the reciprocal effect of each process on all others (with the activity of the Ca^{2+} channels affecting Ca^{2+} concentrations, with Ca^{2+} concentrations affecting both ion channels activity and the extent of muscle contraction, and with the extent of muscle contraction affecting Ca^{2+} concentrations and hence also AP generation), make it impossible to integrate and analyze all of the dynamics by mere thought. A mathematical model that comprehensively and quantitatively integrates all of these dynamics by simulating them all together, can allow the analysis of the inclusive behavior of the entire organ, and of each of its underlying processes.

We hope that following this work, our model's predictions will be examined and verified in the nematode. We also hope that the model itself will be useful to others, either for further inspecting additional questions regarding the *C. elegans* pharynx (which can be done by expanding the model) or for the modeling of other neuro-muscular systems. For these purposes, the detailed solutions of all of the model's PDEs are provided in *SI Appendix*, and the code of our model is also provided (46).

Data, Materials, and Software Availability. Model's code (c++) data have been deposited in GitHub (https://github.com/DanaSherman/CelegansPharynx) (46). All other data are included in the manuscript and/or supporting information.

ACKNOWLEDGMENTS. We thank Nadav Sherman for designing the initial version of the code of both the model and the animation.

1. Z. F. Altun, D. H. Hall, "Alimentary system, pharynx" in *WormAtlas*, L. A. Herndon, Ed. (2009).
2. B. M. Song, L. Avery, Serotonin activates overall feeding by activating two separate neural pathways in Caenorhabditis elegans. *J. Neurosci.* **32**, 1920–1931 (2012).
3. L. Avery, J. H. Thomas, "Feeding and defecation" in *C. elegans II*, D. L. Riddle, T. Blumenthal, B. J. Meyer, J. R. Priess, Eds. (Cold Spring Harbor Laboratory Press, Cold Spring Harbor, NY, ed. 2, 1997).
4. L. Avery, Motor neuron M3 controls pharyngeal muscle relaxation timing in Caenorhabditis elegans. *J. Exp. Biol.* **175**, 283–297 (1993).
5. S. Li, J. A. Dent, R. Roy, Regulation of intermuscular electrical coupling by the Caenorhabditis elegans innexin inx-6. *Mol. Biol. Cell* **14**, 2630–2644 (2003).
6. L. Avery, B. B. Shtonda, Food transport in the C. elegans pharynx. *J. Exp. Biol.* **206**, 2441–2457 (2003).
7. C. Fang-Yen, L. Avery, A. D. T. Samuel, Two size-selective mechanisms specifically trap bacteria-sized food particles in Caenorhabditis elegans. *Proc. Natl. Acad. Sci. U.S.A.* **106**, 20093–20096 (2009).
8. K. Ramakrishnan, P. G. Okkema, Regulation of C. elegans neuronal differentiation by the ZEB-family factor ZAG-1 and the NK-2 homeodomain factor CEH-28. *PLoS One* **9**, e113893 (2014).
9. A. A. Kozlova, M. Lotfi, P. G. Okkema, Cross talk with the GAR-3 receptor contributes to feeding defects in Caenorhabditis elegans eat-2 mutants. *Genetics* **212**, 231–243 (2019).
10. I. R. Brenner, D. M. Raizen, C. Fang-Yen, Pharyngeal timing and particle transport defects in Caenorhabditis elegans feeding mutants. *J. Neurophysiol.* **128**, 302–309 (2022).
11. D. G. Albertson, J. N. Thomson, The pharynx of Caenorhabditis elegans. *Phil. Trans. R. Soc. Lond. B Biol. Sci.* **275**, 299–325 (1976).
12. N. F. Trojanowski, O. Padovan-Merhar, D. M. Raizen, C. Fang-Yen, Neural and genetic degeneracy underlies Caenorhabditis elegans feeding behavior. *J. Neurophysiol.* **112**, 951–961 (2014).
13. N. F. Trojanowski, D. M. Raizen, C. Fang-Yen, Pharyngeal pumping in Caenorhabditis elegans depends on tonic and phasic signaling from the nervous system. *Sci. Rep.* **6**, 22940 (2016).
14. P. Phelan, Innexins: Members of an evolutionarily conserved family of gap-junction proteins. *Biochim. Biophys. Acta* **1711**, 225–245 (2005).
15. N. Azimi Hashemi *et al.*, Rhodopsin-based voltage imaging tools for use in muscles and neurons of Caenorhabditis elegans. *Proc. Natl. Acad. Sci. U.S.A.* **116**, 17051–17060 (2019).
16. B. Shtonda, L. Avery, CCA-1, EGL-19 and EXP-2 currents shape action potentials in the Caenorhabditis elegans pharynx. *J. Exp. Biol.* **208**, 2177–2190 (2005).
17. E. B. Maryon, B. Saari, P. Anderson, Muscle-specific functions of ryanodine receptor channels in Caenorhabditis elegans. *J. Cell Sci.* **111**, 2885–2895 (1998).
18. D. S. Walker, N. J. Gower, S. Ly, G. L. Bradley, H. A. Baylis, Regulated disruption of inositol 1,4,5-trisphosphate signaling in Caenorhabditis elegans reveals new functions in feeding and embryogenesis. *Mol. Biol. Cell* **13**, 1329–1337 (2002).
19. R. Altenberger, K. A. Lindsay, J. M. Ogden, J. R. Rosenberg, The interaction between membrane kinetics and membrane geometry in the transmission of action potentials in non-uniform excitable fibres: A finite element approach. *J. Neurosci. Methods* **112**, 101–117 (2001).
20. A. L. Hodgkin, A. F. Huxley, A quantitative description of membrane current and its application to conduction and excitation in nerve. *J. Physiol.* **117**, 500–544 (1952).
21. E. De Schutter, "Modeling intracellular calcium dynamics" in *Computational Modeling Methods for Neuroscientists*, E. De Schutter, Ed. (The MIT Press, 2009), pp. 93–106.
22. S. N. Yu, P. E. Crago, H. J. Chiel, A nonisometric kinetic model for smooth muscle. *Am. J. Physiol.* **272**, C1025–C1039 (1997).

23. I. Wang *et al.*, A mathematical model of airway and pulmonary arteriole smooth muscle. *Biophys. J.* **94**, 2053–2064 (2008).
24. Z. F. Altun, D. H. Hall, "Muscle system, nonstriated muscle" in *WormAtlas,* L. A. Herndon, Ed. (2009).
25. A. P. Sparacio, N. F. Trojanowski, K. Snetselaar, M. D. Nelson, D. M. Raizen, Teething during sleep: Ultrastructural analysis of pharyngeal muscle and cuticular grinder during the molt in Caenorhabditis elegans. *PLoS One* **15**, e0233059 (2020).
26. M. W. Davis, R. Fleischhauer, J. A. Dent, R. H. Joho, L. Avery, A mutation in the C. elegans EXP-2 potassium channel that alters feeding behavior. *Science* **286**, 2501–2504 (1999).
27. A. Rohatgi, WebPlotDigitizer Software (Version 4.6, Pacifica, CA, 2022). https://automeris.io/WebPlotDigitizer. Accessed 16 February 2023.
28. K. A. Steger, B. B. Shtonda, C. Thacker, T. P. Snutch, L. Avery, The C. elegans T-type calcium channel CCA-1 boosts neuromuscular transmission. *J. Exp. Biol.* **208**, 2191–2203 (2005).
29. M. W. Davis *et al.*, Mutations in the Caenorhabditis elegans Na, K-ATPase alpha-subunit gene, eat-6, disrupt excitable cell function. *J. Neurosci.* **15**, 8408–8418 (1995).
30. C. J. Franks *et al.*, Ionic basis of the resting membrane potential and action potential in the pharyngeal muscle of Caenorhabditis elegans. *J. Neurophysiol.* **87**, 954–961 (2002).
31. R. Y. N. Lee, L. Lobel, M. Hengartner, H. R. Horvitz, L. Avery, Mutations in the α1 subunit of an L-type voltage-activated Ca2 channel cause myotonia in Caenorhabditis elegans. *EMBO J.* **16**, 6066–6076 (1997).
32. R. C. Caylor, Y. Jin, B. D. Ackley, The Caenorhabditis elegans voltage-gated calcium channel subunits UNC-2 and UNC-36 and the calcium-dependent kinase UNC-43/CaMKII regulate neuromuscular junction morphology. *Neural Dev.* **8**, 10 (2013).
33. O. Hobert, "The neuronal genome of Caenorhabditis elegans" in *WormBook*, E. Jorgensen, Ed. (The C. elegans Research Community, WormBook, 2013).
34. R. Fleischhauer *et al.*, Ultrafast inactivation causes inward rectification in a voltage-gated K(+) channel from Caenorhabditis elegans. *J. Neurosci.* **20**, 511–520 (2000).
35. S. Shimozono *et al.*, Slow Ca2+ dynamics in pharyngeal muscles in Caenorhabditis elegans during fast pumping. *EMBO Rep.* **5**, 521–526 (2004).
36. K. R. Norman *et al.*, The Rho/Rac-family guanine nucleotide exchange factor VAV-1 regulates rhythmic behaviors in C. elegans. *Cell* **123**, 119–132 (2005).
37. E. De Schutter, P. Smolen, "Calcium dynamics in large neuronal models" in *Methods in Neuronal Modeling: From Ions to Networks,* C. Koch, I. Segev, Eds. (MIT Press, 1998), pp. 211–246.
38. L. Avery, The genetics of feeding in Caenorhabditis elegans. *Genetics* **133**, 897–917 (1993).
39. D. M. Raizen, L. Avery, Electrical activity and behavior in the pharynx of Caenorhabditis eleguns. *Neuron* **12**, 483–495 (1994).
40. J. T. Chiang, M. Steciuk, B. Shtonda, L. Avery, Evolution of pharyngeal behaviors and neuronal functions in free-living soil nematodes. *J. Exp. Biol.* **209**, 1859–1873 (2006).
41. E. Marder, Electrical synapses: Rectification demystified. *Curr. Biol.* **19**, R34–R35 (2008).
42. A. Destexhe, J. R. Huguenard, "Modeling voltage-dependent channels" in *Computational Modeling Methods for Neuroscientists,* E. De Schutter, Ed. (MIT Press, Cambridge, MA, 2009), pp. 107–138.
43. A. Y. Palyanov, K. V. Samoilova, N. V. Palyanova, EGL-19 and EXP-2 ion channels modelling within C. Elegans pharyngeal muscle cell allows reproduction of CA2+ driven action potentials, both single events and trains. bioRxiv [Preprint] (2017). https://doi.org/10.1101/228650 (Accessed 16 February 2023).
44. A. Senatore, W. Guan, A. N. Boone, J. D. Spafford, T-type channels become highly permeable to sodium ions using an alternative extracellular turret region (S5-P) outside the selectivity filter. *J. Biol. Chem.* **289**, 11952–11969 (2014).
45. L. Avery, H. R. Horvitz, Pharyngeal pumping continues after laser killing of the pharyngeal nervous system of C. elegans. *Neuron* **3**, 473–485 (1989).
46. D. Sherman, "C++ code of *C. elegans* pharynx model". GitHub repository. https://github.com/DanaSherman/CelegansPharynx. Deposited 16 February 2023.